scientific reports

OPEN

Magnetic NH$_2$-MIL-101(Al)/Chitosan nanocomposite as a novel adsorbent for the removal of azithromycin: modeling and process optimization

Ali Azari[1,2], Mohammad Malakoutian[3], Kamyar Yaghmaeain[4], Neemat Jaafarzadeh[5], Nabi Shariatifar[4], Gholamabbas Mohammadi[1], Mahmood Reza Masoudi[1], Reza Sadeghi[1], Sanaz Hamzeh[1] & Hossein Kamani[6✉]

In the present study, the magnetic NH$_2$-MIL-101(Al)/chitosan nanocomposite (MIL/Cs@Fe$_3$O$_4$ NCs) was synthesized and used in the removal of azithromycin (AZT) from an aqueous solution for the first time. The as-synthesized MIL/Cs@Fe$_3$O$_4$ NCs was characterized by SEM, TEM, XRD, FTIR, BET, and VSM techniques. The effect of various key factors in the AZT adsorption process was modeled and optimized using response surface methodology based on central composite design (RSM-CCD). The low value of p-value (1.3101e−06) and RSD (1.873) parameters, along with the coefficient of determination > 0.997 implied that the developed model was well fitted with experimental data. Under the optimized conditions, including pH: 7.992, adsorbent dose: 0.279 g/L, time: 64.256 min and AZT concentration: 10.107 mg/L, removal efficiency and AZT adsorption capacity were obtained as 98.362 ± 3.24% and 238.553 mg/g, respectively. The fitting of data with the Langmuir isotherm (R^2: 0.998, X^2: 0.011) and Pseudo-second-order kinetics (R^2: 0.999, X^2: 0.013) showed that the adsorption process is monolayer and chemical in nature. ΔH° > 0, ΔS° > 0, and ΔG° < 0 indicated that AZT removal was spontaneous and endothermic in nature. The effect of Magnesium on AZT adsorption was more complicated than other background ions. Reuse of the adsorbent in 10 consecutive experiments showed that removal efficiency was reduced by about 30.24%. The performance of MIL/Cs@Fe$_3$O$_4$ NCs under real conditions was also tested and promising results were achieved, except in the treatment of AZT from raw wastewater.

In the last decades, the removal of antibiotics has received more attention from researchers due to their cumulative properties, high toxicity, chemical stability, biological activity, and the development of bacterial resistance even in small amounts[1]. So far, a variety of antibiotics including macrolides, tetracyclines, and chloramphenicols are found in environmental media[2]. Azithromycin ($C_{38}H_{72}N_2O_{12}$, AZT) is a broad-spectrum macrolide antibiotic with a long half-life that is primarily used to treat respiratory, enteric, and genitourinary infections[3,4]. The presence of azithromycin in a water body is usually related to personal hygiene products, pharmaceutical industry waste, hospital waste, therapeutic drugs, animal husbandry, agriculture, and aquaculture. The presence of trace amounts of AZT in drinking water is a public health concern because little is known about the potential chronic health effects associated with the long-term ingestion of mixtures of these compounds through drinking water[5]. Moreover, AZT antibiotic residues can alter the human microbiome and cause health disturbances, such as allergic reactions, chronic toxic effects after prolonged exposure, and disruption of digestive system functions[6]. On the other side, due to their extensive usage and negligible human metabolism, about 30–90%

[1]Sirjan School of Medical Sciences, Sirjan, Iran. [2]Student Research Committee, Sirjan School of Medical Sciences, Sirjan, Iran. [3]Department of Environmental Health Engineering, School of Public Health, Kerman University of Medical Sciences, Kerman, Iran. [4]Department of Environmental Health Engineering, School of Public Health, Tehran University of Medical Sciences, Tehran, Iran. [5]Department of Environmental Health Engineering, School of Public Health, Jondishapour University of Medical Sciences, Ahvaz, Iran. [6]Health Promotion Research Center, Zahedan University of Medical Sciences, Zahedan, Iran. ✉email: azari.hjh@gmail.com

1

of AZT antibiotics are excreted unchanged in the body of humans and animals as active compounds in urine and feces[7,8]. Environmental exposure to active pharmaceutical ingredients (APIs) can have negative effects on the health of ecosystems and humans[9]. Therefore, effective removal of AZT antibiotics from wastewater before their discharge is inevitable and necessary. Conventional wastewater treatment processes are not usually able to remove pharmaceutical compounds[10].

Among various wastewater treatment processes, adsorption is considered as a promising and widely-used technique for removing pharmaceutical substances from wastewater due to its flexible design, ease of operation, and cost-effectiveness[11,12]. Nevertheless, the development of affordable, high-performance and reusable adsorbents for the pharmaceutical wastewater treatment remains a challenge among researchers and requires more comprehensive studies. MOFs are organic–inorganic hybrid crystalline porous structures consist of metal complex or cluster joined by organic ligands. MOFs have unique properties such as large pore volumes, adjustable pore size, fine tunable pore surface property, low density, flexible framework and alterable pore functionalities, flexibility in chemistry design, pore size, shape, and structure and high affinity to polymers and environmental friendly[13,14]. As reported in the literature, MOFs are widely used in many fields such as electrocatalysis, electrochemical devices (fuel cells, electrolysis cells, batteries, supercapacitors, sensors, etc.), gas storage and separation, liquid separation and purification, catalysis, and sensing[15]. MOFs are usually synthesized through the self-linkage and coordination of metallic species with organic ligands in a cyclic frame with porosity[16,17].

MIL_{Al}-101 is a representative of the broad family of MOFs, which is characterized by high porosity, stability, easy preparation, low cost, and surface functionality, making it an ideal choice for adsorption of contaminants[18]. Many researchers have proved the excellent performance of MILs toward the adsorptive removal of ibuprofen[19], toxic dyes[20], sulfacetamide[21] and ciprofloxacin[22]. Although MOFs-based adsorbents provide some advantages, however, their tendency to aggregate and lose during the recovery process is considered a respective drawback for their applications[23]. Chitosan (Cs) is a natural, non-toxic, and inexpensive polysaccharide that with its unique physical and chemical properties including biocompatibility, biodegradability, flexibility, and various functional groups[24], has been proposed as a substrate to prevent MOF agglomeration/aggregation in the present study. Furthermore, the presence of free hydroxyl and amino groups in chitosan structure and permission of their chemical modification can facilitate the adsorption of various types of pollutants in chitosan-derived nanocomposites[25]. Therefore, it is expected that the combination of extraordinary properties of chitosan and MIL_{Al}-101 for the synthesis of MIL/Cs NCs as a novel adsorbent will have an acceptable performance toward AZT removal. After synthesis of MIL/Cs NCs and their utilization in the removal of AZT from samples, separation and reuse of the adsorbent is necessary and inevitable to reduce the costs of the adsorption process. This process is generally performed with filtration and centrifugation which require a lot of time, cost, and manpower. Hence, induction of magnetic properties to the MIL/Cs NCs using Fe_3O_4 NPs and its separation using an external magnet was considered to solve this problem[26,27].

Given the issues mentioned above, the purpose of present research can be summarized as follows: (a) Synthesis of novel MIL/Cs@Fe_3O_4 NCs and its characterization by SEM, TEM, XRD, FTIR, BET and VSM techniques, (b) Modeling and optimization of the AZT adsorption using response surface methodology based central composite design (RSM-CCD), (c) study of isotherms, kinetics and thermodynamics of process, (d) Investigation of the interfering anion presence on the performance of adsorption process, (e) Determination of MIL/Cs@Fe_3O_4 NCs desorption and their stability and, (f) Comparison of synthesized adsorbent ability to remove AZT in real conditions with laboratory conditions.

Materials and methods

Materials and equipment.
Reagents and instruments used in this study were given in Supplementary Information, Text 1.

Preparation and characterization of adsorbents.
Chitosan obtained from shrimp shell (Cs). The chitosan (Cs) synthesis procedure in detail is provided on Supplementary Information, Text 2.

NH_2-MIL_{Al}-101. NH_2-MIL_{Al}-101 was synthesized by a microwave method in accordance with a previously reported procedure with some modifications[28]. In detail, 0.51 g of $AlCl_3$·$6H_2O$ and 0.56 g of 2-aminoterephthalic acid were dissolved in 70 mL of DMF. After 30 min stirring, the mixture was placed in a Teflon*-lined autoclave and heated at 140 °C by microwave for 3 h. Afterwards the autoclave was allowed to naturally cool to room temperature. The resulting solid product was filtered and washed with acetone for several times, activated with methanol under reflux over-night and evacuated at 200 °C for 6 h.

NH_2-MIL_{Al}-101/chitosan (MIL/Cs NCs). The procedure for the synthesis of NH_2- MILAl-101/chitosan as described by Wang et al.[18], was applied with slight modifications. 0.3 g chitosan powders, 1.1 g 2-aminoterephthalic acid, and 0.89 g $AlCl_3$·$6H_2O$ were mixed well and dispersed in 100 mL DMF. The mixture was stirred for 45 min before being introduced into a Teflon autoclave, followed the same procedure as that for synthesis of NH_2-MIL_{Al}-101.

NH_2-MIL_{Al}-101/chitosan@Fe_3O_4 (MIL/Cs@Fe_3O_4 NCs). MIL/Cs@Fe_3O_4 NCs was prepared by co-precipitation under alkaline conditions following our previous published method[29]. 0. 5 g of MIL/Cs NCs was added in 400 mL of iron salt solution consisting of iron (II) chloride (0.03 M) and iron (III) chloride (0.06 M). The obtained mixture was homogenized using an US probe for 30 min (20 kHz, 585 W). Under US irradiation, 30 mL of NaOH solution added drop wise into the mixture until pH kept at 10–11. The suspension was mixed and heated at 80 °C for 1 h followed by cooling. Finally, the obtained black solid was magnetically collected and

Factor	Name	Units	Minimum	Maximum	coded low	Coded high	Mean	Std. Dev	
A	pH		2	10	4	8	6	1.79	
B	Adsorbent dose	g/L	0.1	0.5	0.2	0.4	0.3	0.09	
C	Time	min	10	90	30	70	50	17.89	
D	AZT Conc	mg/L	10	50	20	40	30	8.94	
		Factor 1	Factor 2	Factor 3	Factor 4	Response			
		A	B	C	D	Adsorption efficiency	Predicted efficiency	Remain concentration	Adsorption capacity
Std	Run	*	g/L	min	mg/L	%	%	mg/L	mg/g
14	1	8	0.2	30	40	85.00	84.26	6.00	170.00
3	2	6	0.3	10	30	55.37	56.45	13.39	55.37
4	3	6	0.3	50	30	73.78	72.56	7.87	73.78
7	4	6	0.3	50	50	47.70	48.10	26.15	79.50
18	5	10	0.3	50	30	97.79	98.19	0.66	97.79
19	6	8	0.4	70	20	94.65	94.58	1.07	47.33
17	7	6	0.5	50	30	69.95	70.35	9.02	41.97
11	8	4	0.2	30	20	30.36	29.62	13.93	30.36
9	9	6	0.3	50	30	75.00	72.56	7.50	75.00
2	10	6	0.3	50	30	71.00	72.56	8.70	71.00
20	11	6	0.3	50	30	73.00	72.56	8.10	73.00
16	12	4	0.2	70	20	41.07	41.00	11.79	41.07
21	13	6	0.1	50	30	53.52	53.92	13.94	160.55
8	14	8	0.2	70	40	82.29	82.22	7.08	164.58
12	15	4	0.4	30	40	41.49	40.75	23.40	41.49
1	16	6	0.3	50	30	70.00	72.56	9.00	70.00
10	17	6	0.3	90	30	72.00	71.73	8.40	72.00
13	18	4	0.4	70	40	49.16	49.09	20.34	49.16
5	19	8	0.4	30	20	82.43	81.69	3.51	41.21
6	20	6	0.3	50	10	80.23	80.63	1.98	26.74
15	21	2	0.3	50	30	23.44	23.84	22.97	23.44

Table 1. CCD matrix ranges and their response for adsorption of AZT by MIL/Cs@Fe_3O_4.

washed several times with distilled water until pH became neutral. MIL/Cs@Fe_3O_4 NCs was dried overnight at 105 °C in a hot air oven and stored in an airtight container for further experiments.

Characterization.   Characteristic analyzes for the synthesized adsorbent are presented in Supplementary Information, Text 3.

Adsorption procedures.   In this study, all the experiments were performed in a 250 mL conical flask containing 100 mL of aqueous solution. To determine the effect of key parameters on the removal efficiency, the sample solutions were agitated in an air shaker at 150 rpm at room temperature. A Central Composite Design (Four factorial CCD) approach in the series of batch tests were developed to optimize the critical parameters in adsorption process (an experimental matrix of the RSM-CCD is listed in Table 1). All experiments were performed in triplicate. The adsorption efficiency (R, %), and capacity (qe, mg/g), were calculated by the following equations:

$$R = \frac{(C_0 - C_e)}{C_0},$$ (1)

$$qe = \frac{(C_0 - C_e)}{m} \times V,$$ (2)

where C_0 (mg/L) and C_e (mg/L) are the initial and equilibrium AZT concentrations, respectively; V (L) is the volume of solution, and m (g) is the mass of adsorbent. After optimizing the above-mentioned parameters, kinetics (0–80 min), isotherms (10–200 mg/L) and thermodynamic (278–343 °K) of adsorption process were investigated according to a study by Azari et al.[30]. Desorption and economic feasibility of MIL/Cs@Fe_3O_4 NCs toward AZT removal were investigated with ultrasound + chemical modifications in various ethanol concentrations. Finally, effect of background electrolytes on adsorption process and adsorbent performance in real samples was investigated and reported.

Adsorption modeling by CCD-DF. To enhance the AZT removal efficiency using the smallest number of potential adsorption tests, a response surface methodology (RSM) based central composite design (CCD) technique (MODDE® Pro Software, V.11.0.2) was applied. Table 1 shows the proposed statistical method to investigate the effect of four independent parameters including pH (2–10), adsorbent dose (0.1–0.5 g/L), AZT concentration (10–50 mg/L) and time (10–90 min) on the response factor (adsorption efficiency, %). In this study, a total of 21 experiments were investigated. At a level of 0.05, ANOVA analysis was used to discover which factors had a significant impact on the response variable. The model parameters were described using analysis of variance (ANOVA), correlation coefficient (R^2) value, F-test value, and contrasting of experimental Vs. model-predicted data. The model's accuracy and applicability were further evaluated using the probability value (Prob > F), relative standard deviation (RSD), pure error, and Q^2 value. The operational parameters of the AZT adsorption process were optimized using desirability functions (DF). The selected models' process optimization findings were repeated (n = 5) on a laboratory scale (actual circumstances) until the best and most accurate model for AZT adsorption was found.

Results and discussion

Adsorbent characteristics. The SEM analysis of the MIL/Cs@Fe_3O_4 NCs is shown in Fig. 1a. As shown, NH_2-MIL_{Al}-101 with hexagonal shape and average diameter of 88.5 ± 10.1 nm are distributed non-uniformly on the surface of chitosan. The surface of chitosan is observed as smooth, sheet-like and layered form. In other sides, Fe_3O_4 NPs with spherical structure (23.3 ± 4.0 nm) are observable on the chitosan surface. The image reveals that the surface of the adsorbent is rough and has a good porosity. This feature leads to a better contact of the adsorbent with the pollutant, which resulted in an improvement in adsorption performance. Furthermore, no agglomeration is seen in the MIL/Cs@Fe_3O_4 NCs structure which can be related to the presence of chitosan in the structure of the synthesized sample. A TEM analysis was applied to investigate the shape and particle sizes of MIL/Cs@Fe_3O_4 NCs, and its results are presented in Fig. 1b. The images indicate that the NH_2-MIL_{Al}-101 and Fe_3O_4 nanoparticles are hexagonal and spherical respectively and distributed heterogeneously in a size range of 80–100 nm and 20–40 nm on the chitosan surface, which coincides with results obtained from SEM image. Due to the higher density of NH_2-MIL_{Al}-101 and Fe_3O_4 than chitosan, these nanoparticles are recognized in a darker color (black), while chitosan has a light and transparent structure. DLS technique was employed to determine the particle size distribution (Figure is not shown): the obtained average sizes of Fe_3O_4 NPs, NH_2-MIL_{Al}-101 and MIL/Cs@Fe_3O_4 NCs were 21.75 nm, 85.34 nm and 108.96 nm, respectively. The FTIR spectrum of the adsorbents at a wavelength within 400–4000 cm⁻¹ is shown in Fig. 1c. The peak at 609 cm⁻¹ is attributed to the Fe–O vibration of Fe_3O_4 NPs[31]. The medium peak at 466 cm⁻¹ is due to Al–O vibrations, which confirms the formation of the organometallic structure. The broad peak from 3382 cm⁻¹ is attributed to the –NH_2 and –OH groups and the peaks at 1689 and 1598 cm⁻¹ are related to the $CONH_2$ and NH_2 groups in the chitosan structure, respectively[32]. The peaks at 1438 and 1496 cm⁻¹ were assigned to symmetric and asymmetric stretching of carboxyl groups, respectively. The peak at 1393 and 771 cm⁻¹ correspond to the –COO– bond and C–H vibration of the aromatic cycles in the phenyl ring. These bonds at 1438, 1496, 1393 and 771 cm⁻¹ suggest the presence of the organic ligands of 2-aminoterephthalic acid. Two peaks appearing at 1259 and 1116 cm⁻¹ can be attributed to the stretching vibrations of aromatic functional epoxy C–O and alkoxy C–O groups, respectively. XRD pattern of synthesised MIL/Cs@Fe_3O_4 NCs in the range of 2θ = 5–70° is represented in Fig. 1d. The characteristic peaks of NH_2-MIL_{Al}-101 are appeared at 2θ = 6.28°, 7.12°, 8.89°, 10.27° and 17°, which were relatively similar to the patterns of previous references[33,34]. The diffraction peaks at 10.96°, 19.86° and 21.64° are assigned to crystal forms of chitosan. On the other hand, the obtained peaks at 26.3°, 30.22°, 35.57°, 43.21°, 53.57°, 62.74°, and 65.88° related to the diffraction planes of 172°, 220°, 342°, 400°, 511°, 122°, and 106°, respectively confirm the presence of Fe_3O_4 crystals in the MIL/Cs@Fe_3O_4 NCs structure (0866-088-01 JCPDS NO.). The above results indicate that NH_2-MIL_{Al}-101 and Fe_3O_4 NPs are loaded onto the CS and MIL/Cs@Fe_3O_4 NCs was synthesized successfully. Magnetic measurements and separation of MIL/Cs@Fe_3O_4 NCs were taken with a VSM analysis at room temperature, as presented in Fig. 1e. This analysis was performed in a magnetic field of ± 10 KOe and saturation magnetization around ± 80 emu/g. The results showed that the saturation magnetization (Ms) of MIL/Cs@Fe_3O_4 NCs was observed around 60.77 emu/g. The result clearly demonstrated the appropriate magnetic property of the synthesized adsorbent. The Nitrogen adsorption–desorption isotherms and the pore size distribution of the MIL/Cs@Fe_3O_4 NCs is shown in Fig. 1f and Supplementary Table S1. The isotherms are identified as type IV with H_4 typical hysteresis loops, which are the characteristic isotherm of mesoporous materials according to IUPAC classification. The BET surface area and average pore diameters of the of the product were also calculated as 451.73 m²/g and 2.78 nm, respectively. The BET surface area calculated for the MIL/Cs@Fe_3O_4 NCs is ~ 1.5 times higher than the Fe_3O_4@C nanocomposite synthesized by Van Tran et al.[35]. Although these values are higher than all samples (Fe_3O_4 NPs, NH_2-MIL_{Al}-101 and MIL/Cs NCs), but this difference between MIL/Cs@Fe_3O_4 NCs and MIL/Cs NCs is not too large. This phenomenon may be due to the occupation of the porosity of MIL/Cs NCs by magnetic nanoparticles (Fe_3O_4) and/or clotting (agglomeration) of the nanocomposite. Thermal stabilities of MIL/Cs@Fe_3O_4 NCs were investigated by using TGA analysis (Fig. 1g). MIL/Cs@Fe_3O_4 NCs showed gradual weight loss within three steps. The first step occurred in the temperature range of 50–250 °C with a weight loss of 7%, attributed to the evaporation of solvent or water molecules inside the framework. A weight loss of 20% in the temperature range of 150–440 °C could be ascribed to the decomposition of guest molecules or unreacted products inside the ligand structure. In the final step, beyond 440 °C, MIL/Cs@Fe_3O_4 NCs structure degraded. The thermal stability results revealed the good stability of the synthesized adsorbent.

AZT removal under different systems. Figure 2 shows the ability of MIL/Cs@Fe_3O_4 NCs compared to Cs, Fe_3O_4, NH_2-MIL_{Al}-101 and MIL/Cs NCs for AZT removal under similar experimental conditions (experi-
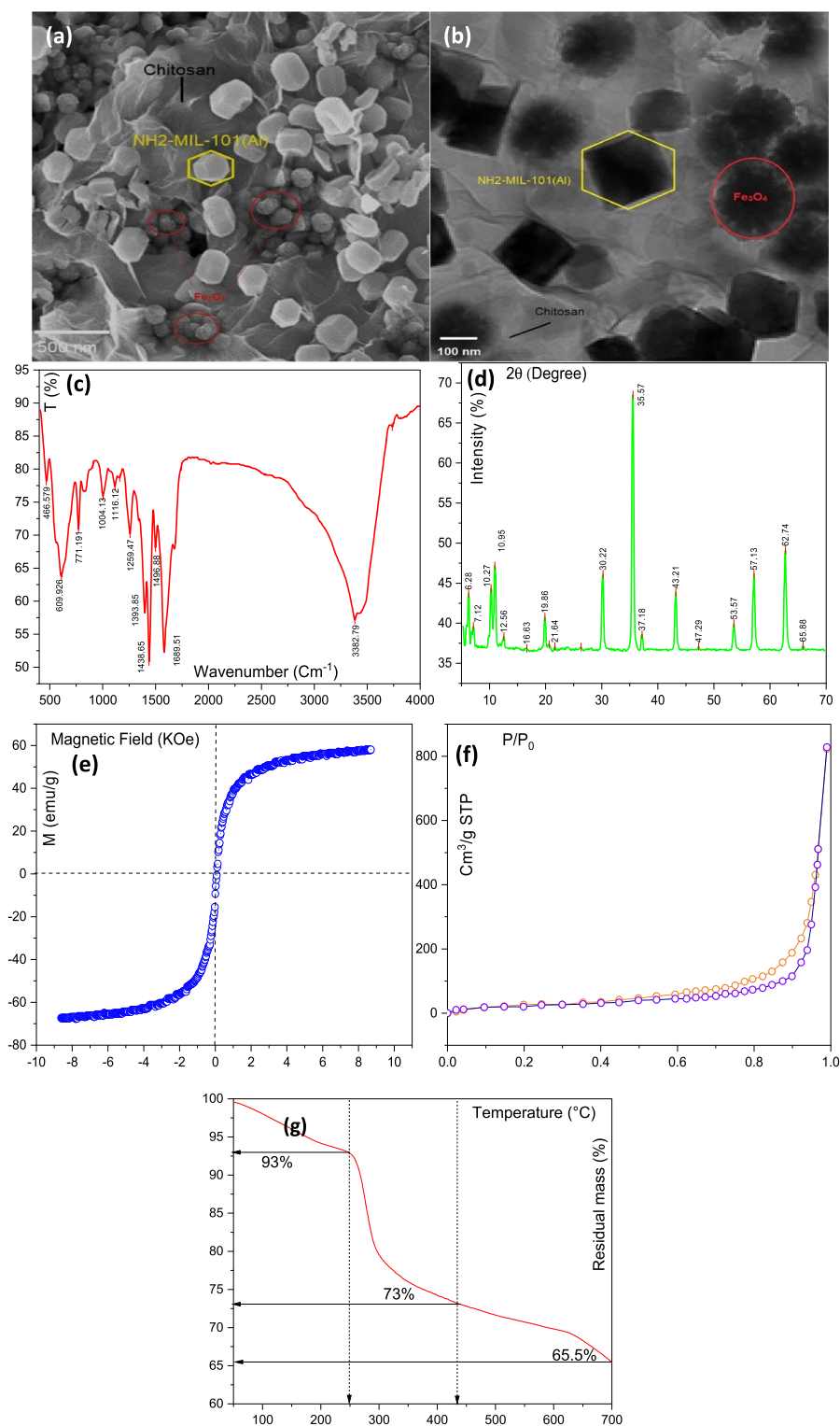
Figure 1. SEM (**a**), TEM (**b**), FTIR (**c**), XRD (**d**), VSM (**e**), BET (**f**) and TGA (**g**) analysis of MIL/Cs@Fe_3O_4 NCs.

ment conditions: Contact time: 60 min, pH: 7 ± 0.4, Sample dose: 0.5 g/L, AZT Conc.: 50 mg/L). AZT removal efficiencies by Cs and Fe_3O_4 were negligible (33.43 and 28%, respectively), showing that AZT cannot be effectively removed by Cs and Fe_3O_4. However, higher removal efficiencies were observed when Cs and Fe_3O_4 were coupled with NH_2-MIL_{Al}-101 i.e., MIL/Cs NCs and MIL/Cs@Fe_3O_4 NCs. The removal efficiencies of AZT by NH_2-MIL_{Al}-101, MIL/Cs NCs and MIL/Cs@Fe_3O_4 NCs were 44.23, 57.54 and 73.21% within 60 min, respectively. Higher surface area, better average pore volume/ size and more functional groups seem to be the reasons
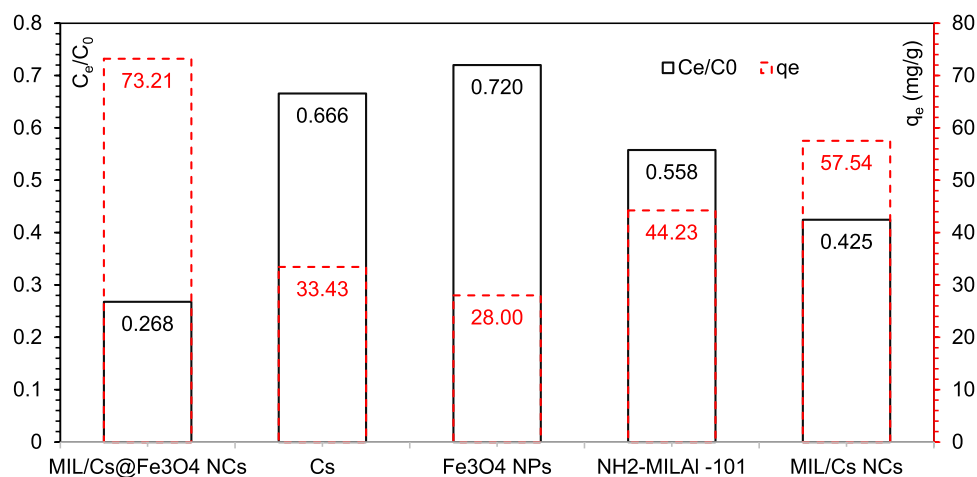
Figure 2. Comparison of AZT removal with different adsorbents under same conditions.

for the superior performance of MIL/Cs@Fe$_3$O$_4$ NCs over other adsorbents. The priority and order of samples in AZT removal were obtained as MIL/Cs@Fe$_3$O$_4$ NCs > MIL/Cs NCs > NH$_2$-MIL$_{Al}$-101 > Cs > Fe$_3$O$_4$, respectively. Accordingly, MIL/Cs@Fe$_3$O$_4$ NCs was selected as the preferred adsorbent in AZT removal and was used in following experiments.

Effect of key parameters on adsorption of AZT. The effect of pH changes in the range of 2 to 10 on AZT adsorption by MIL/Cs@Fe$_3$O$_4$ NCs was investigated. As can be seen from Fig. 3, the removal efficiency is improved by increasing the pH so that the highest efficiency is observed in alkaline conditions and the lowest was obtained at pH < 5. In other side, the point of zero charge (pH$_{pzc}$) values for MIL/Cs@Fe$_3$O$_4$ NCs was obtained to be 4.6 (Supplementary Fig. S1). The increasing trend of AZT removal with increasing the pH of the solution can be associated with the fact that pHpzc (4.6) of adsorbent is lower than the pKa (8.7) of AZT (pH$_{pzc}$ < pH < pKa). Therefore, at pH = ~8, the surface charges of the adsorbent and the adsorbate become opposites charge and an electrostatic attraction occurs between them which results in maximum adsorption. As a result, the optimal pH 8 was employed in further adsorption tests. Imani poor et al. (2021) studied the adsorption of azithromycin onto L-methionine modified montmorillonite K10 and 3-aminopropyltriethoxysilane functionalized magnesium phyllosilicate organoclays. They found that the maximum adsorption capacity obtained at a pH 8.0 ± 0.1[36]. A similar result was observed for azithromycin removal using powdered zeolites in research by Sousa et al.[37]. They reported that the lowest efficiency was recorded under acidic pH (2.5–4.5), while alkaline conditions improved the performance of the azithromycin adsorption process. The effects of adsorbent dosage (from 0.1 to 0.5 g/L) on adsorption of AZT by MIL/Cs@Fe$_3$O$_4$ NCs was investigated at pH = 8.0, contact time = 60 min, and room temperature. Based on the results, the increase in the adsorbent dose has led to an increase in adsorption efficiency from 53 to 76%. The specific surface area and large quantity of reactive surface centers or functional groups of the adsorbent towards contaminates might be associated to adsorption percentage improvement as adsorbent increases[38,39]. Wahab et al. found that increasing the amount of magnetic activated carbon (MAC) from 0.01 to 0.15 g can increase the removal efficiency of AZT from ~ 10 to 100%[40]. In azithromycin adsorption onto modified natural clinoptilolite, Saadi et al. observed a direct relationship between process effectiveness and adsorbent dose. They reported that the initial quick adsorption was attributed to the unoccupied site and surface area of absorbent, resulting in successful adsorbate diffusion within the adsorbent[41]. The adsorption of AZT on MIL/Cs@Fe$_3$O$_4$ NCs was studied by adjusting contact time in the optimized pH and adsorbent dosage. From Fig. 3, increasing the contact time from 10 to 90 min has resulted in a 20% improvement in efficiency. Efficiency improvements with increasing time can be due to increase the contact and collisions of AZT with the MIL/Cs@Fe$_3$O$_4$ NCs, which subsequently improves the mass transfer of contaminates on to the adsorbent. Adsorbents generally have a limited and specific adsorption capacity and become saturated after reaching equilibrium time. The proper efficiency at the beginning of the adsorption process can be linked to the existence of large unoccupied sites and functional groups on the adsorbents that begin to fill over time[42]. A more detailed about the effect of contact time on azithromycin adsorption has been discussed and reported in the kinetics study section. Balarak et al. investigated the effect of contact time on AZT molecule adsorption on Azolla Filiculoides-based activated porous carbon ranging from 0 to 150 min. They found that increasing the contact time leads to an increase in percentage removal[43]. Other researchers have observed similar results in the adsorption of different antibiotics by modified alpha alumina nanoparticles and NaY zeolite synthesized from wheat straws ash[44,45]. Increasing the initial concentrations from 10 to 50 mg/L has resulted in a considerable drop in efficiency, as seen in Fig. 3. The inverse relationship between AZT concentration and efficiency is owed to the saturation of accessible active sites on MIL/Cs@Fe$_3$O$_4$ NCs. On the contrary, increasing the initial concentration of AZT has led to an increase in adsorbate per mass of adsorbent (qe, mg/g). The increased in qe (mg/g) at higher concentrations might be explained by the significant driving force for mass exchange at a large initial concentration[46]. Davoodi et al. studied the removal of AZT using raw and saponin-modified nano diatomite by varying the initial AZM
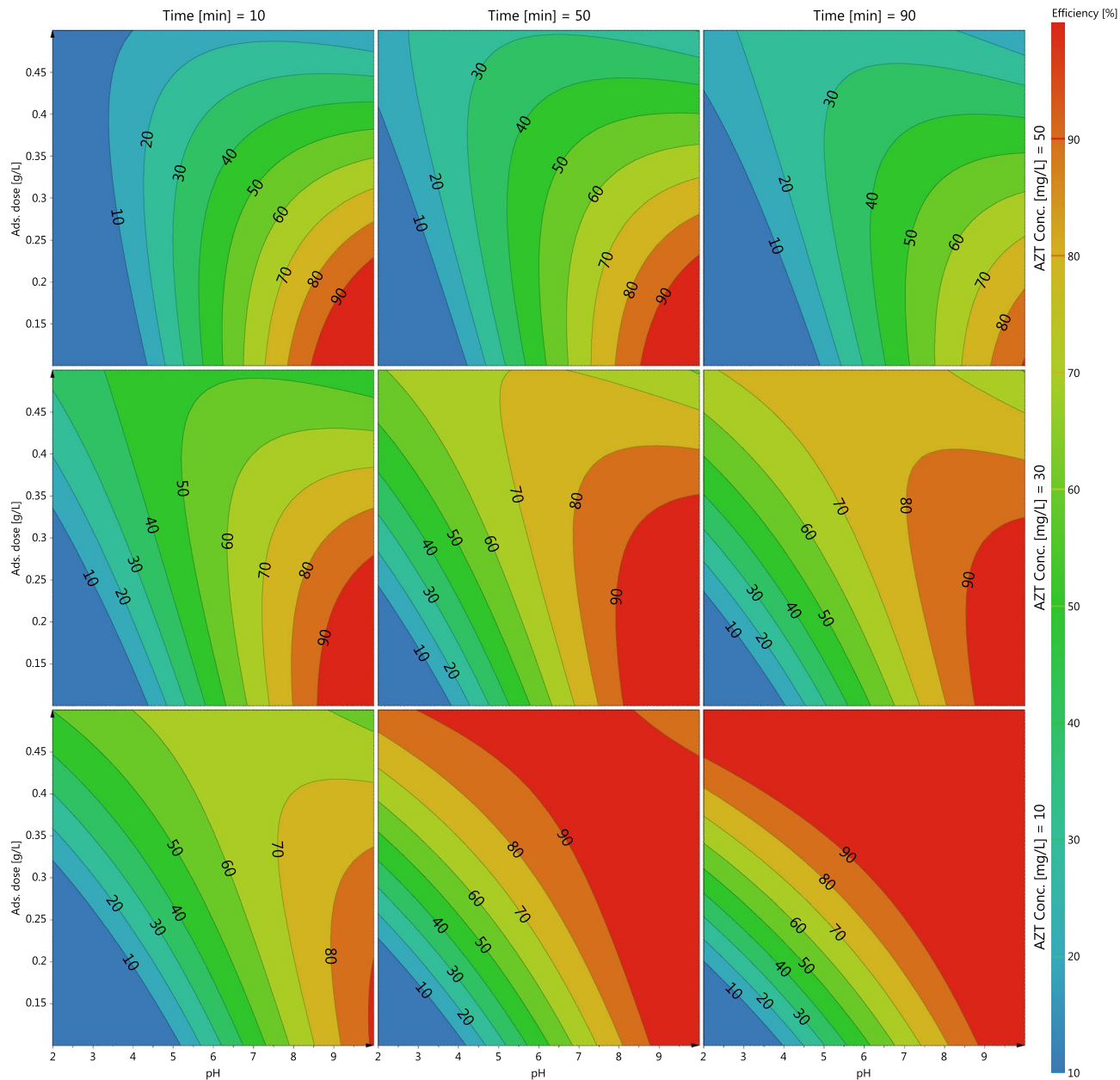
Figure 3. 4D plots of variables effect on AZT removal.

concentration from 20 to 100 mg/L. They noticed that increasing the pollutant concentration causes a significant reduction in the adsorption process[47]. In 2020, Ardakani et al. used from PECVD film to evaluate the influence of initial concentration on AZT removal[48]. According to the Ardakani report's, increasing the AZT concentration from 0 to 160 mg/L has resulted in a decrease in efficiency, and the highest efficiency has been obtained in the lowest concentration. Rapid saturation of active sites with increasing pollutant concentration was the main cause of efficiency reduction.

Statistical analysis and modeling of AZT adsorption. The validity of the model and operational parameters was investigated by RSM-CCD technique and ANOVA analysis. Table 2 summarizes the ANOVA results for the selected model. The developed model can well describe and predicted the adsorption of AZT by MIL/Cs@Fe$_3$O$_4$ NCs, as evidenced by the high values of R^2 (> 0.997), Adj R^2 (> 0.991), and Model F-value (170.46). Furthermore, the R^2 value has reasonably agreed with the Adjusted R^2 value; i.e., the difference is lesser than 0.2. On the other hand, RSD (1.873) confirms the model's suitability for interpreting the studied process. The signal-to-noise ratio is expressed by the adequate precision (A–P) parameter. This value was found to be 46.973 (A–P > 4) which indicates an adequate signal and model could be used to navigate the design (good match between experimental and computed results)[49]. The p-value of the lack of fit parameter was 6.2431e−01 (greater than 0.05), indicating that the developed model was appropriate and the predicted values are accurate[50].

Model statistics						
Removal	**DF**	**SS**	**MS**	**F-value**	**p-value**	**SD**
Total	21	9.7665e+04	4.6507e+03			
Constant	1	8.9274e+04	8.9274e+04			
Total corrected	20	8.3912e+03	4.1956e+02			2.0483e+01
Model	14	8.3702e+03	5.9787e+02	1.7046e+02	**1.3101e−06**	2.4451e+01
Residual	6	2.1044e+01	3.5074e+00			1.8728e+00
Lack of Fit	2	4.4166e+00	2.2083e+00	5.3122e−01	**6.2431e−01**	1.4860e+00
Pure error	4	1.6628e+01	4.1570e+00			2.0389e+00
Q^2	0.949			A–P	46.9730	
R^2	0.997			RSD	1.873	
R^2 adj	0.992			Predicted R^2	0.9486	
Parameters statistics						
	SS	**MS**	**F-value**	**p-value**	**Effect**	
pH	2.7639E+03	2.7639E+03	7.8802E+02	< 0.0001	74.349	
Ads. dose	1.3494E+02	1.3494E+02	3.8470E+01	8.0000E−04	16.4282	
Time	2.3371E+02	2.3371E+02	6.6630E+01	2.0000E−04	15.2875	
AZT Conc	5.2904E+02	5.2904E+02	1.5084E+02	< 0.0001	− 32.5281	
pH*Ads. dose	3.4674E+02	3.4674E+02	9.8860E+01	< 0.0001	− 74.4833	
pH*Time	9.8000E+00	9.8000E+00	2.7900E+00	1.4570E−01	− 8.8535	
pH*AZT Conc	9.2730E−01	9.2730E−01	2.6440E−01	6.2550E−01	3.85191	
Ads. dose*Time	1.7700E+01	1.7700E+01	5.0500E+00	6.5800E−02	11.9001	
Ads. dose*AZT Conc	7.0550E+01	7.0550E+01	2.0120E+01	4.2000E−03	− 33.5981	
Time*AZT Conc	4.0360E+01	4.0360E+01	1.1510E+01	1.4600E−02	− 17.9681	
pH ^{2}	2.0894E+02	2.0894E+02	5.9570E+01	2.0000E−04	− 23.0822	
Ads. dose ^{2}	1.7034E+02	1.7034E+02	4.8560E+01	4.0000E−04	− 20.8412	
Time ^{2}	1.1244E+02	1.1244E+02	3.2060E+01	1.3000E−03	− 16.9331	
AZT Conc.^{2}	1.0520E+02	1.0520E+02	2.9990E+01	1.5000E−03	− 16.3786	
Optimization process						
Factor	**Value**	**Unit**	**RSD**	**Contribution**	**Failure**	**DF**
pH	7.992	*	–	64.0637		
Ads. dose	0.279	g/L		20.1934		
Time	64.256	min	–	1.20639	4%	0.996
AZT Conc	10.107	mg/L	–	14.5365		
Efficiency	98.362	%	± 3.24	100		
Repeat (n = 5)	96.021	%	± 4.23	*		

Table 2. Analysis of variance (ANOVA) for CCD modeling and process optimization results.

Variance analysis was also used to investigate the effects of variables. The results show that all parameters had a considerable influence on the AZT adsorption except interaction between pH and time, pH and AZT concentration and adsorbent dose and time. The equation in terms of actual factors can be used to make predictions about the response for given levels of each factor. The equation of AZT adsorption on MIL/Cs@Fe_3O_4 NCs can be defined as follows:

$$
\begin{aligned}
\text{Efficiency}(\%) = {}& 72.56 + 18.59(\text{pH}) + 4.11(\text{Ads.dose}) + 3.82(\text{Time}) - 16.26(\text{AZTConc.}) - 9.31(\text{pH} \times \text{Ads.dose}) \\
& - 1.11(\text{pH} \times \text{Time}) + 0.963(\text{pH} \times \text{AZTConc.}) + 1.49(\text{Ads.dose} \times \text{Time}) \\
& - 8.40(\text{Ads.dose} \times \text{AZTConc.}) - 4.49(\text{Time} \times \text{AZTConc.}) - 2.89(\text{pH})^2 \\
& - 2.61(\text{Ads.dose}) - 2.12(\text{Time}) - 8.19(\text{AZTConc.})^2
\end{aligned}
$$

(3)

It can be seen that the pH, Ads.dose**,** Time, pH × AZTConc. and Ads.dose × Time parameters have positive signs, and the others are negative. These findings show that increasing the mentioned factors has a synergistic effect on the adsorption process; nevertheless, increasing other parameters reduces the efficiency. According to Eq. (3) and Table 2, pH with the highest coefficient has the greatest impact on the AZT adsorption process by MIL/Cs@Fe_3O_4 NCs. Plotting actual data Vs. predicted data with $R^2 > 0.948$ illustrated that the developed model has a strong ability to predict removal efficiency (Supplementary Fig. S2a). The normal probability plot of the studentized residuals (Supplementary Fig. S2b), shows that the plotted points are close to a straight line (balanced and uniform distribution of residuals around the normalcy line.) that indicates the model has been well

Isotherms					
Model	**Equation**	**Nomenclature**	**Parameters**	**Values**	**X^2**
Langmuir	$C_e/q_e = C_e/Q_m + 1/K_a Q_m$	The slope and intercept of the linear plot of C_e/q_e versus C_e give Q_m and K_a, respectively	Q_m (mg g^{-1})	238.5527	0.011
			K_L (L mg^{-1})	0.19614	
			R_L	0.1812	
			R^2	0.9981	
Freundlich	$\ln q_e = (1/n) \ln C_e + \ln K_F$	The slope and intercept of the linear plot of $\ln q_e$ versus $\ln C_e$ give $1/n$ and K_F, respectively	n	3.3661	0.024
			K_F (L mg^{-1})	60.837	
			R^2	0.9759	
Temkin	$q_e = B_l \ln C_e + B_l \ln K_T$	B_l and K_T are calculated from the slope and intercept of the linear plot of q_e against $\ln C_e$, respectively	B_l	32.0417	0.031
			K_T (L mg^{-1})	10.04241	
			R^2	0.9396	
Dubinin and Radushkevich	$\ln q_e = -K\varepsilon^2 + \ln Q_s, (\varepsilon = RT \ln (1+1/C_e))$	The slope and intercept of the linear plot of $\ln q_e$ versus ε^2 give K and Q_s, respectively	E (kJ mol^{-1})	2704.0065	0.046
			D (mol^{-2} kJ^{-2})	6.8384E−08	
			R^2	0.7093	
Kinetics					
Model	**Equation**	**Nomenclature**	**Parameters**	**Values**	**X^2**
Pseudo-first-order	$\ln (q_e - q_t) = -k_1 t + \ln(q_e)$	The slope and intercept of the linear plot of $\ln (q_e - q_t)$ versus t give k_1 and q_e, respectively	k_1 (min^{-1})	0.000157474	0.032
			q_e (mg/g)	82.49361895	
			R^2	0.9833	
Pseudo-second-order	$t/q_t = t/q_e + 1/(k_2 q_e)^2$	The slope and intercept of the linear plot of t/q_t versus t give q_e and k_2, respectively	k_2 (g mg^{-1} min^{-1})	0.035565425	0.013
			q_e (mg/g)	37.6004392	
			R^2	0.9991	
Intraparticle diffusion	$q_t = K_{diff} t^{1/2} + C$	The slope and intercept of the linear plot of q_t versus $t^{1/2}$ give K_{diff} and C, respectively	K_{dif} (g mg^{-1} min-0.5)	7.988476742	0.024
			C	5.621384922	
			R^2	0.9979	
Elovich	$q_t = 1/\beta \ln(t) + 1/\beta \ln(\alpha\beta)$	β and α are obtained from the slope and intercept of the plot of q_t versus $\ln (t)$, respectively	β (g mg^{-1})	9.950388641	0.039
			α (g mg^{-1} min^{-1})	0.029242544	
			R^2	0.9543	
Thermodynamic					
Temperature	**ln k_d**	**ΔS° (kJ/mol K)**	**ΔG° (kJ/mol)**	**ΔH° (kJ/mol)**	**qe**
278 °K	3.5		− 8.08		32.68
288 °K	4.15		− 9.94		34.29
298 °K	5.37	0.22	− 13.31	755.23	35.63
328 °K	6.58		− 17.95		36.05
343 °K	8.01		− 22.85		36.18

Table 3. Isotherm, kinetic and thermodynamic parameters for adsorption of AZT onto MIL/Cs@Fe$_3$O$_4$ NCs NCS adsorbent.

fitted with the experimental results. Supplementary Fig. S2c shows the residuals are randomly scattered near the horizontal zero reference (± 3) indicating a good fit of the model for AZT adsorption by MIL/Cs@Fe$_3$O$_4$ NCs.

Process optimization. After determination of the effect of each parameter (positive and negative roles) on the adsorption process, calculating the optimum conditions is essential and inevitable[51]. The purpose of optimization was improvement of AZT adsorption efficiency in the batch process, so the response parameter (AZT adsorption efficiency) was set to maximum level to determine the best performance of system. The lower and upper limit values of other variables were taken from the experimental data ranges (see Table 1). Based on the DF approach results, the maximum adsorption efficiency for AZT was 98.362 ± 3.24% at pH = 7.992, AZT conc. = 10.107 mg/L, ads. dose g/L = 0.279 and time equal to 64.256 min. To determine the accuracy of the software model results, optimized conditions (the above result) were simulated in laboratory scale and repeated 5 times. The evidence suggested that the simulated test results (96.021 ± 4.23%) are consistent with the model's results (98.362 ± 3.24%), so the result recorded by DF was used were used in the isotherms, kinetics and thermodynamic investigation. The percentage of parameters participation in maximizing the AZT adsorption process also revealed that pH and time with 64.063 and 1.206%, had the highest and lowest impact on system optimization, respectively.

Adsorption isotherms. To determine the best-fitting isotherm model with experimental data, the Langmuir, Freundlich, Temkin, and Dobbin-Radoshkvich models were studied (conditions: pH = 7.992, AZT

Conc. = 10.107 mg/L, Ads. dose g/L = 0.279). From Table 3 and Supplementary data, Fig. S3, The R^2 value for the Langmuir isotherm ($R^2 > 0.9981$) is higher than other models (0.9759, 0.9396, and 0.7093 for Freundlich, Temkin, and Dobbin-Radoshkvich, respectively), indicating that experimental data is in well agreement with Langmuir model. The lower value of χ^2 error (0.011) also confirms the results obtained. According to the Langmuir model, the AZT is adsorbed in a monolayer on a homogeneous surface of adsorbent with uniform energies for all the binding sites without any interaction between the molecules[52,53]. The adsorption capacity upon the Langmuir model was obtained as 238.5527 mg of AZT per gram of MIL/Cs@Fe$_3$O$_4$ NCs. The dimensionless separation factor (RL) of the Langmuir adsorption isotherm was used to determine the favourability of the adsorption process (irreversible → RL = 0, favourable → 0 < RL < 1, linear → RL = 1 and unfavourable → RL > 1). All the RL values lie in the range of 0 < RL < 1, which suggests that the AZT are favourably adsorbed on MIL/Cs@Fe$_3$O$_4$ NCs. Compared to Langmuir isotherm model, Freundlich isotherm model had the poorest fit with experimental data, as determined by comparison of R^2 and χ^2 values. However, high values of k_F (60.837 L mg^{-1}) and n parameter (greater than 1) indicated that adsorption of adsorbate on adsorbent was acceptable/feasible[54,55]. Table 3 reveals that the experimental data are less consistent with the Temkin isotherm model than either of the previous two models. Nevertheless, the positivity of Temkin isotherm constants (B = 32.042) proves that the adsorption process in the present study is endothermic in nature. The results indicated that experimental data fitted with the D–R isotherm with $R^2 > 0.709$ under the optimized condition. Magnitude of adsorption energy, E, for AZT adsorption on the MIL/Cs@Fe$_3$O$_4$ NCs adsorbent was calculated to be 2704.0065 kJ/mol (> 40 kJ/mol), representing that the adsorption is chemisorption process[56,57]. Non-linear results of the studied isotherms (Fig. S3e) also clearly showed compliance of the experimental data with the Langmuir isotherm.

Adsorption kinetics. As can be seen from the Supplementary data, Fig. S4e, the adsorption efficiency increased sharply at the initial 60 min of the experiment, whereas negligible changes were observed thereafter, which indicates that the adsorption process has reached equilibrium state. The high adsorption rate at the beginning of process may be explained by the high affinity of MIL/Cs@Fe$_3$O$_4$ NCs for trapping pollutants due to the huge number of vacant sites (active sites) on adsorbent. Over time, the active sites in the adsorbent structure are occupied (filled) by pollutant molecules, which results in reduced efficiency and rate of AZT adsorption[58,59]. In the following, four conventional kinetic models including pseudo-first-order, pseudo-second-order, Elovich, and intraparticle diffusion, were employed to investigate the kinetics of AZT adsorption on MIL/Cs@Fe$_3$O$_4$ NCs under optimized conditions (see Supplementary data, Fig. S4a–d). Furthermore, the parameters related to the kinetic models i.e., error functions, and regression correlation coefficients (R^2), are listed in Table 3. A pseudo-first-order model was found to be in good agreement with experimental data with a high $R^2 > 0.983$, and χ^2 values less than 0.032. Higher R^2 values (0.9991) and lower χ^2 rate (0.013) on the one hand and more compatibility between experimental qe (qe,exp: 35.86 mg/g) with the calculated qe (qe,cal: 37.60 mg/g) on the other hand clearly indicated that the pseudo-second-order model better describe the adsorption behaviour of AZT onto MIL/Cs@Fe$_3$O$_4$ NCs. The error values ($\chi^2 = 0.039$) and R^2 parameter (0.9543) obtained from the Elovich model indicate that there is the least agreement between the experimental data and this model, and Elovich model is not suitable for describing the experimental data compared to the previous two models. The results obtained so far confirmed that the dominant mechanism of adsorption process is chemisorption[60]. The results also depicted that intraparticle diffusion model with $R^2 > 0.997$ and $\chi^2 = 0.024$ has a higher ability than pseudo-first-order and Elovich models in interpreting data, while it has a weaker performance than pseudo-second-order kinetic model. Besides, the resulting fitting line in the intraparticle diffusion plot (q_t against $t^{0.5}$) did not pass through the origin. This shows that intraparticle diffusion was a rate-controlling step (rate-limiting mechanism) in the AZT adsorption process, along with the chemisorption reaction[61,62].

Adsorption thermodynamic. Supplementary data, Fig. S5a shows the effect of different temperatures on the AZT adsorption efficiency at the obtained optimized conditions. As it turns out, with increasing temperature from 278 to 343 °K, adsorption capacities improved from 32.68 to 36.18 mg/g. For evaluating feasibility and nature of AZT adsorption process on MIL/Cs@Fe$_3$O$_4$ NCs, the thermodynamic parameters i.e., Gibbs free energy ($\Delta G°$), enthalpy change ($\Delta H°$), and entropy change ($\Delta S°$) were investigated and their results are given in Table 3. The quantities of enthalpy and entropy were calculated from slope and intercept of the plot of ln ln K_d vs. 1/T (Van't Hoff plot, Supplementary data, Fig. S5b). The values of $\Delta H°$ and $\Delta S°$ were found to be 755.23 and 0.22 kJ/mol, respectively. Positive value of $\Delta H°$ and also the directed trend between ln K_d and temperature implied that AZT adsorption on the MIL/Cs@Fe$_3$O$_4$ NCs was endothermic in nature, indicating that higher temperature enhanced adsorption capacity. $\Delta S°$ value became positive, so the increased randomness can be expected at the solid/solution interface during AZT adsorption. Besides, positive $\Delta S°$ value corresponded to an increase in the freedom degree of the adsorbed species[63]. Negative values of $\Delta G°$ (− 8.08 to − 22.85 kJ/mol) indicated feasibility and spontaneous nature of adsorption process. Moreover, the degree of spontaneity was increased by increasing temperature.

Effect of background ions. The effect of background electrolytes at an initial concentration of 1, 10 and 20 mM on AZT adsorption by MIL/Cs@Fe3O4 NCs are shown Fig. 4. It was found that the Na$^+$ and K$^+$ cations had a smaller effect on antibiotic adsorption than Mg^{2+} and Ca^{2+} ions. This might be explained by the fact that the high polarization power of divalent ions caused them to exert a stronger squeezing-out effect. The following reasons are also given by the researchers: (a) A dense water hydration shell might surround the adsorbed Mg^{2+} and Ca^{2+} ions could hinder the available adsorption sites by blocking the hydrophobic adsorption region, and (b) It is possible that Mg^{2+} and Ca^2 compete directly for adsorption sites on MIL/Cs@Fe$_3$O$_4$ NCs due to inner-sphere complexation, which inhibits the formation of charge-assisted H-bonds with antibiotics.
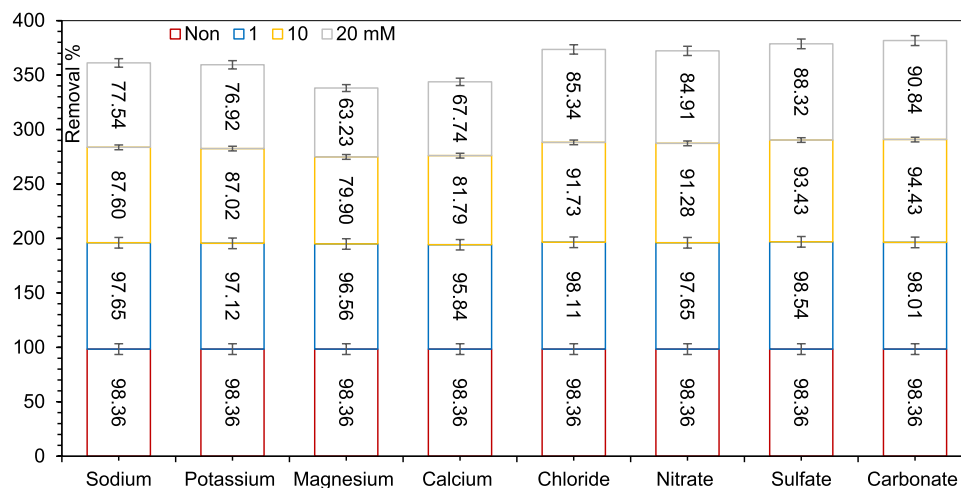
Figure 4. Effect of interfering ions on the efficiency of AZT adsorption under optimized conditions.

AZT adsorption by MIL/Cs@Fe$_3$O$_4$ NCs was not significantly affected by background anions, including Cl$^-$, NO$_3^-$, SO$_4^{2-}$ and CO$_3^{2-}$, which may be due to the strong repellence/repulsion between anions and the negatively charged adsorbent surface[64].

Desorption and stability. To investigate the desorption and economic feasibility of MIL/Cs@Fe$_3$O$_4$ NCs toward AZT removal, the adsorbent was recycled with ultrasound + chemical modifications in various ethanol concentrations ranging from 10 to 100 (v/v percent). Figure 5a shows the amount of desorption against time at various ethanol concentrations under optimized conditions. As shown, the desorption percentage rose dramatically at various ethanol concentrations and reached to equilibrium in 40 min. In Fig. 5a,b, it can also be seen that the efficiency (%), capacity (mg/g) and rate (k, based on pseudo-second order kinetic) of desorption process have an upward trend up to the ethanol concentrations of 75%, but after that no further improvement has been observed. In the following, the adsorbent's reusability was evaluated for 10 consecutive cycles. For this purpose, after each cycle, MIL/Cs@Fe$_3$O$_4$ NCs were washed with ethanol and distilled water (75% v/v). As observed from Fig. 5c, the removal efficiency has decreased by only 9.13% during the first to fifth cycles, and this reduction in the adsorption has reached 30.24% in the tenth cycle. The decrease in efficiency can be ascribed to the loss of adsorbent mass and the filling of active sites or functional groups of the adsorbent during repeated runs. The amounts of leached aluminium and iron were 0.024 and 0.147 mg/L in the first cycle, and fell to 0.009 and 0.11 mg/L in the tenth cycle. The leaching of Al and Fe amounts in repeated runs is reasonable (Less than the water standard level), which proves the stability and durability of MIL/Cs@Fe$_3$O$_4$ NCs for AZT treatment.

Adsorption mechanism. The mechanism of organic compounds' adsorption is usually described by hydrogen bonding, electrostatic interaction, and π–π interaction. MIL/Cs@Fe$_3$O$_4$ NCs used in this study are enriched with π-electrons, amino group (–NH$_2$), and acidic carboxyl group (–COOH) that can play an important role in the adsorption mechanism between MIL/Cs@Fe$_3$O$_4$ NCs and AZM through hydrogen bonding (H-bonds), electrostatic interaction, and π–π interactions. As can be seen in Fig. S6, AZM is surrounded by high amounts of –OH, –CH$_3$, =O, –O–, –N–, –N=, and –OCH$_3$ functional groups. The aforementioned functional groups can play a role in AZM adsorption as follows: (a) –OH involved to form hydrogen bonding, (b) =O, –O–, –N–, –N=, and –O–CH$_3$ groups involve in anionic electrostatic interactions, and (c) –CH$_3$ group participates in cationic electrostatic interactions. Figure 6 shows possible adsorption interactions between AZM and MIL/Cs@Fe$_3$O$_4$ NCs. Since there is no π-electron in AZM, it is unlikely to have π–π interactions with MIL/Cs@Fe$_3$O$_4$ NCs[65]. Based on the evidence, adsorption may occur as a result of cationic and anionic electrostatic interactions and H-bonding between AZM and MIL/Cs@Fe$_3$O$_4$ NCs.

Study of real samples. In order to evaluate the effectiveness and potential of the MIL/Cs@Fe$_3$O$_4$ NCs for AZT adsorption in real conditions, a series of experiments on tap water, surface runoff, raw wastewater, and secondary effluent were considered under optimized conditions (AZT concentration spiked: 10 mg/L). In Supplementary data, Table S2, the specifications of samples are listed. As can be seen, all samples have lower efficiency compared to DI-water. For example, the efficiency in tap water was 90.45% while the adsorbent performance in surface runoff, raw and treated wastewater were 85.34%, 48.45%, and 65%, respectively (Supplementary data, Fig. S7). The decrease in AZT adsorption efficiency can be attributed to the presence of TDS, various ions, organic compounds, and other contaminants in the actual samples. Based on the results, it can be reported that MIL/Cs@Fe$_3$O$_4$ NCs has an acceptable ability to remove AZT from aqueous samples under real conditions, although this performance has been significantly reduced in raw wastewater samples.
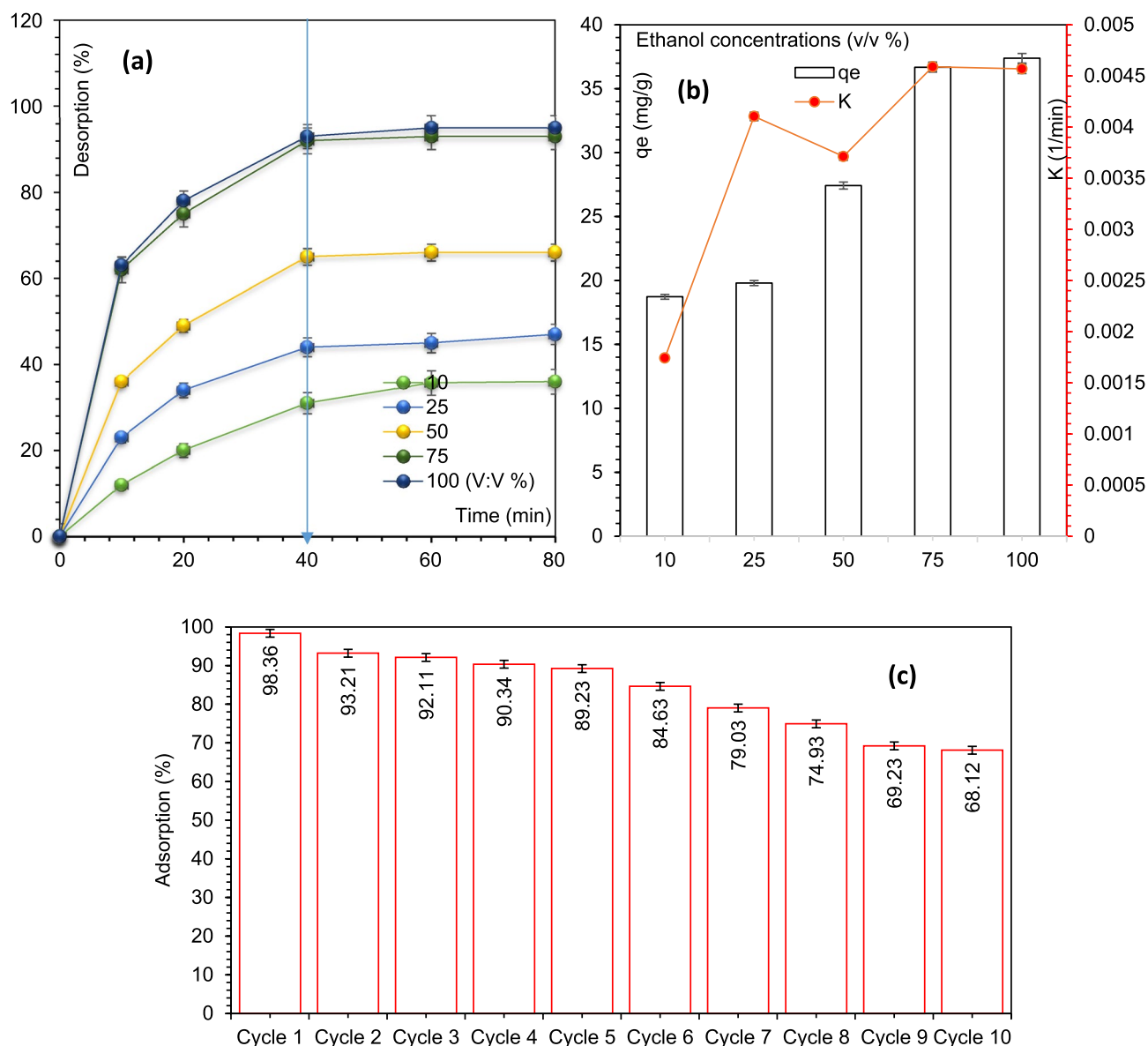
Figure 5. Desorption percentage of AZT at different ethanol concentration (**a**), desorption capacity and the rate of desorption under various ethanol concentrations (**b**) and reusability of MIL/Cs@Fe₃O₄ NCs after AZT treatment for 10 cycles (**c**).

Comparison with previous research. The qm parameter of synthesized adsorbent (adsorption capability based on the Langmuir isotherm model, mg/g) was compared with similar literature in terms of adsorbent type, and the results are summarized in Table 4. It was observed that the MIL/Cs@Fe₃O₄ NCs adsorbent showed good ability to compete with similar systems for treatment of AZT and has the proper place among the literature. It should be noted that the differences between the adsorption capacities in the various adsorbents can be related to the type of materials used (due to variability in size, surface area, number of active sites, and functional groups), adsorbent dosage and the concentration of the AZT in experiments. Available evidence confirms that the adsorbent synthesized in the present study can have a suitable and promising performance in the removal of AZT as a representative of macrolide antibiotics.

Conclusions

Magnetic NH₂-MIL-101(Al)/Chitosan nanocomposite (MIL/Cs@Fe₃O₄ NCs) adsorbent was synthesized and developed for AZT treatment from queues solution. RSM-CCD approach was applied to predict and optimize the effect of key factors on AZT removal. This research led to the following results: (1) he results of ANOVA test revealed that the effect of all parameters on the performance of the AZT adsorption was significant with $Prob > F < = 0.05$ except pH × Time, pH × AZT concentration and Adsorbent dose × Time, (2) The higher adsorption efficiency (predicted: 98.362%, Real: 96.021) is obtained at pH = 7.992, adsorbent dose = 0.279 g/L, time = 64.256 min and the initial concentration = 10.107 mg/L with DF = 0.996, (3) The isotherms and kinetics
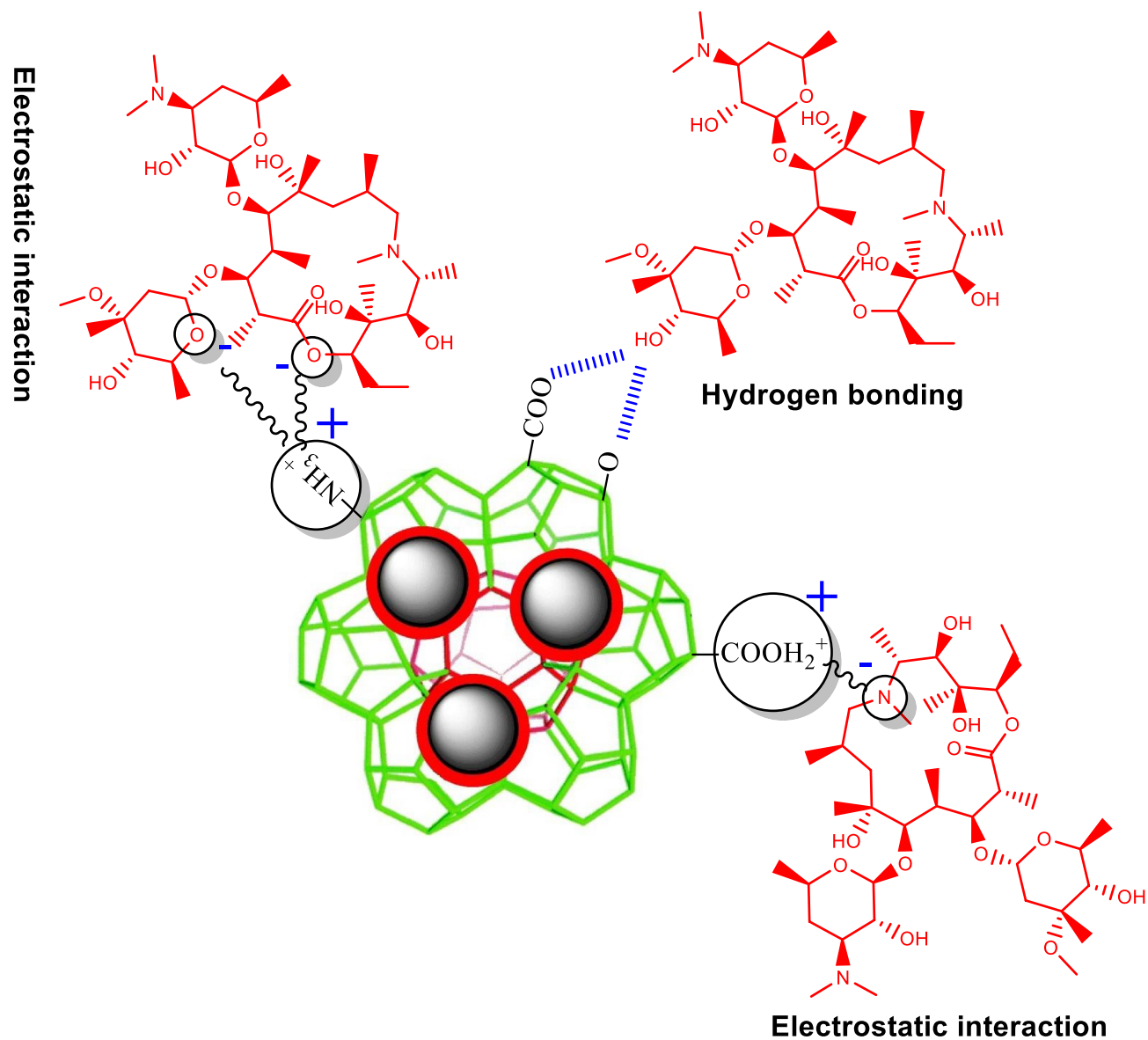
Figure 6. Possible mechanism of AZM adsorption on MIL/Cs@Fe$_3$O$_4$ NCs.

Adsorbent	C$_0$ (mg/L)	Time (min)	Dose (g/L)	q$_m$ (mg/g)	Isotherm	Kinetic	References
ZnO/Si	15	45	0.025	213.32	L	PSO	[48]
Raw nano diatomite	100	60	2.5	68	L	–	[47]
Saponin modified nano diatomite	100	3	1	91.7	L	–	[47]
LMP clay	50	90	0.5	298.78	F	PSO	[36]
AMP clay	50	90	0.5	286.10	F	PSO	[36]
FAU-1	10	30	0.1	8.50	F	PSO	[37]
MIL/CS@Fe$_3$O$_4$ NCS	10.107	64.256	0.279	238.55	L	PSO	This study

Table 4 . Comparison of AZT adsorption reported in the literature with the proposed systems. *L* Langmuir, *F* Freundlich, *PSO* Pseudo-second-order.

of data were best fitted with the Langmuir and pseudo-second-order models, (4) Positive value of ΔH° and negative value of ΔG° indicated that AZT adsorption process was spontaneous and endothermic in nature, (5) After 10 reuses of the MIL/Cs@Fe$_3$O$_4$ NCs, the AZT removal efficiency dropped from 98.36 to 68.12, and (6) The inhibition effect of background electrolytes on AZT adsorption by MIL/Cs@Fe3O4 NCs follows a trend of $Mg^{2+} > Ca^{2+} > K^+ = Na^+ > NO_3^- > Cl^- > SO_4^{2-} > CO_3^{2-}$.

Data availability

The data that support the findings of this study are available from the first author, [Ali Azari], on special request. Part of the data and materials are also available within supplementary materials.

References

1. Yuan, Q. et al. Migration, transformation and removal of macrolide antibiotics in the environment: A review. Environ. Sci. Pollut. Res. **29**, 1–18 (2022).
2. Naraginti, S., Yu, Y.-Y., Fang, Z. & Yong, Y.-C. Visible light degradation of macrolide antibiotic azithromycin by novel ZrO2/Ag@ TiO₂ nanorod composite: Transformation pathways and toxicity evaluation. Process Saf. Environ. Prot. **125**, 39–49 (2019).
3. Tiwari, B. et al. Review on fate and mechanism of removal of pharmaceutical pollutants from wastewater using biological approach. Bioresour. Technol. **224**, 1–12 (2017).
4. Spielmeyer, A. Occurrence and fate of antibiotics in manure during manure treatments: A short review. Sustain. Chem. Pharm. **9**, 76–86 (2018).
5. Rivera-Utrilla, J., Sánchez-Polo, M., Ferro-García, M. Á., Prados-Joya, G. & Ocampo-Pérez, R. Pharmaceuticals as emerging contaminants and their removal from water. A review. Chemosphere **93**, 1268–1287 (2013).
6. Polianciuc, S. I., Gurzău, A. E., Kiss, B., Ştefan, M. G. & Loghin, F. Antibiotics in the environment: Causes and consequences. Med. Pharm. Rep. **93**, 231 (2020).
7. Jelić, A., Gros, M., Petrović, M., Ginebreda, A. & Barceló, D. Occurrence and elimination of pharmaceuticals during conventional wastewater treatment. In Emerging and Priority Pollutants in Rivers, 1–23 (2012).
8. Almeida, A. et al. Human and veterinary antibiotics used in Portugal—A ranking for ecosurveillance. Toxics **2**, 188–225 (2014).
9. Bhushan, P., Gautam, D., Kumar, P., Shukla, S. & Mohan, D. An overview of human health risk from opium alkaloids and related pharmaceutical products pollution in aquatic ecosystems. In Ecological Significance of River Ecosystems, 1–14 (2022).
10. Eniola, J. O., Kumar, R., Barakat, M. & Rashid, J. A review on conventional and advanced hybrid technologies for pharmaceutical wastewater treatment. J. Clean. Prod. **356**, 131826 (2022).
11. Zdarta, J., Meyer, A. S., Jesionowski, T. & Pinelo, M. Multi-faceted strategy based on enzyme immobilization with reactant adsorption and membrane technology for biocatalytic removal of pollutants: A critical review. Biotechnol. Adv. **37**, 107401 (2019).
12. Mesdaghinia, A. et al. Removal of phthalate esters (PAEs) by zeolite/Fe₃O₄: Investigation on the magnetic adsorption separation, catalytic degradation and toxicity bioassay. J. Mol. Liq. **233**, 378–390 (2017).
13. Dehghankar, M., Mohammadi, T., Moghadam, M. T. & Tofighy, M. A. Metal-organic framework/zeolite nanocrystal/polyvinylidene fluoride composite ultrafiltration membranes with flux/antifouling advantages. Mater. Chem. Phys. **260**, 124128 (2021).
14. Van Tran, T. et al. High performance of Mn2 (BDC) 2 (DMF) 2-derived MnO@ C nanocomposite as superior remediator for a series of emergent antibiotics. J. Mol. Liq. **308**, 113038 (2020).
15. Kuppler, R. J. et al. Potential applications of metal-organic frameworks. Coord. Chem. Rev. **253**, 3042–3066 (2009).
16. Shah, S. S. A. et al. Recent advances on oxygen reduction electrocatalysis: Correlating the characteristic properties of metal organic frameworks and the derived nanomaterials. Appl. Catal. B **268**, 118570 (2020).
17. Van Tran, T. et al. Hexagonal Fe-based MIL-88B nanocrystals with NH2 functional groups accelerating oxytetracycline capture via hydrogen bonding. Surf. Interfaces **20**, 100605 (2020).
18. Wang, Y., Wang, K., Lin, J., Xiao, L. & Wang, X. The preparation of nano-MIL-101 (Fe)@ chitosan hybrid sponge and its rapid and efficient adsorption to anionic dyes. Int. J. Biol. Macromol. **165**, 2684–2692 (2020).
19. Xiong, P., Zhang, H., Li, G., Liao, C. & Jiang, G. Adsorption removal of ibuprofen and naproxen from aqueous solution with Cu-doped Mil-101 (Fe). Sci. Total Environ. **797**, 149179 (2021).
20. Vo, T. K., Trinh, T. P., Nguyen, V. C. & Kim, J. Facile synthesis of graphite oxide/MIL-101 (Cr) hybrid composites for enhanced adsorption performance towards industrial toxic dyes. J. Ind. Eng. Chem. **95**, 224–234 (2021).
21. Zhou, Q. & Liu, G. Urea-functionalized MIL-101 (Cr)@ AC as a new adsorbent to remove sulfacetamide in wastewater treatment. Ind. Eng. Chem. Res. **59**, 12056–12064 (2020).
22. Li, Z. et al. Efficiently removal of ciprofloxacin from aqueous solution by MIL-101 (Cr)-HSO 3: The enhanced electrostatic interaction. J. Porous Mater. **27**, 189–204 (2020).
23. Li, X. et al. Water contaminant elimination based on metal–organic frameworks and perspective on their industrial applications. ACS Sustain. Chem. Eng. **7**, 4548–4563 (2019).
24. Nasrollahzadeh, M., Shafiei, N. & Orooji, Y. Magnetic chitosan stabilized Cu (II)-tetrazole complex: An effective nanocatalyst for the synthesis of 3-imino-2-phenylisoindolin-1-one derivatives under ultrasound irradiation. Sci. Rep. **12**, 1–13 (2022).
25. Nasrollahzadeh, M., Sajjadi, M., Iravani, S. & Varma, R. S. Starch, cellulose, pectin, gum, alginate, chitin and chitosan derived (nano) materials for sustainable water treatment: A review. Carbohyd. Polym. **251**, 116986 (2021).
26. Hemmati, S., Heravi, M. M., Karmakar, B. & Veisi, H. In situ decoration of Au NPs over polydopamine encapsulated GO/Fe₃O₄ nanoparticles as a recyclable nanocatalyst for the reduction of nitroarenes. Sci. Rep. **11**, 1–14 (2021).
27. El-Sharkawy, R. M., Swelim, M. A. & Hamdy, G. B. Aspergillus tamarii mediated green synthesis of magnetic chitosan beads for sustainable remediation of wastewater contaminants. Sci. Rep. **12**, 1–15 (2022).
28. Ma, X.-H., Yang, Z., Yao, Z.-K., Xu, Z.-L. & Tang, C. Y. A facile preparation of novel positively charged MOF/chitosan nanofiltration membranes. J. Membr. Sci. **525**, 269–276 (2017).
29. Moazzen, M. et al. Multi-walled carbon nanotubes modified with iron oxide and silver nanoparticles (MWCNT-Fe₃O₄/Ag) as a novel adsorbent for determining PAEs in carbonated soft drinks using magnetic SPE-GC/MS method. Arab. J. Chem. **12**, 476–488 (2019).
30. Azari, A., Nabizadeh, R., Mahvi, A. H. & Nasseri, S. Magnetic multi-walled carbon nanotubes-loaded alginate for treatment of industrial dye manufacturing effluent: Adsorption modelling and process optimisation by central composite face-central design. Int. J. Environ. Anal. Chem. 1–21 (2021).
31. Van Tran, T. et al. Effect of thermolysis condition on characteristics and nonsteroidal anti-inflammatory drugs (NSAIDs) absorbability of Fe-MIL-88B-derived mesoporous carbons. J. Environ. Chem. Eng. **7**, 103356 (2019).
32. Tang, Z. et al. Synthesis of SiBNC-Al ceramics with different aluminum contents via polymer-derived method. J. Am. Ceram. Soc. **105**, 2914–2924 (2022).
33. Aljaddua, H. I., Alhumaimess, M. S. & Hassan, H. M. CaO nanoparticles incorporated metal organic framework (NH2-MIL-101) for Knoevenagel condensation reaction. Arab. J. Chem. **15**, 103588 (2022).
34. Guan, Y., Xia, M., Wang, X., Cao, W. & Marchetti, A. Water-based preparation of nano-sized NH2-MIL-53 (Al) frameworks for enhanced dye removal. Inorg. Chim. Acta **484**, 180–184 (2019).
35. Van Tran, T. et al. Recyclable Fe₃O₄@ C nanocomposite as potential adsorbent for a wide range of organic dyes and simulated hospital effluents. Environ. Technol. Innov. **20**, 101122 (2020).

36. Imanipoor, J., Mohammadi, M. & Dinari, M. Evaluating the performance of L-methionine modified montmorillonite K10 and 3-aminopropyltriethoxysilane functionalized magnesium phyllosilicate organoclays for adsorptive removal of azithromycin from water. *Sep. Purif. Technol.* **275**, 119256 (2021).

37. de Sousa, D. N. R. *et al.* Equilibrium and kinetic studies of the adsorption of antibiotics from aqueous solutions onto powdered zeolites. *Chemosphere* **205**, 137–146 (2018).

38. Li, X. *et al.* Adsorption materials for volatile organic compounds (VOCs) and the key factors for VOCs adsorption process: A review. *Sep. Purif. Technol.* **235**, 116213 (2020).

39. Dehghani, M. H., Salari, M., Karri, R. R., Hamidi, F. & Bahadori, R. Process modeling of municipal solid waste compost ash for reactive red 198 dye adsorption from wastewater using data driven approaches. *Sci. Rep.* **11**, 1–20 (2021).

40. Wahab, M. *et al.* Adsorption-membrane hybrid approach for the removal of azithromycin from water: An attempt to minimize drug resistance problem. *Water* **13**, 1969 (2021).

41. Saadi, Z., Fazaeli, R., Vafajoo, L., Naser, I. & Mohammadi, G. Promotion of clinoptilolite adsorption for azithromycin antibiotic by Tween 80 and Triton X-100 surface modifiers under batch and fixed-bed processes. *Chem. Eng. Commun.* **208**, 328–348 (2021).

42. Mahmoudian, M. H., Fazlzadeh, M., Niari, M. H., Azari, A. & Lima, E. C. A novel silica supported chitosan/glutaraldehyde as an efficient sorbent in solid phase extraction coupling with HPLC for the determination of Penicillin G from water and wastewater samples. *Arab. J. Chem.* **13**, 7147–7159 (2020).

43. Balarak, D., Mahvi, A. H., Shahbaksh, S., Wahab, M. A. & Abdala, A. Adsorptive removal of azithromycin antibiotic from aqueous solution by azolla filiculoides-based activated porous carbon. *Nanomaterials* **11**, 3281 (2021).

44. Nguyen, N. T., Dao, T. H., Truong, T. T., Nguyen, T. M. T. & Pham, T. D. Adsorption characteristic of ciprofloxacin antibiotic onto synthesized alpha alumina nanoparticles with surface modification by polyanion. *J. Mol. Liq.* **309**, 113150 (2020).

45. Ali, M. M. M. & Ahmed, M. J. Adsorption behavior of doxycycline antibiotic on NaY zeolite from wheat (*Triticum aestivum*) straws ash. *J. Taiwan Inst. Chem. Eng.* **81**, 218–224 (2017).

46. Dovi, E. *et al.* Functionalization of walnut shell by grafting amine groups to enhance the adsorption of Congo red from water in batch and fixed-bed column modes. *J. Environ. Chem. Eng.* **9**, 106301 (2021).

47. Davoodi, S., Dahrazma, B., Goudarzi, N. & Gorji, H. G. Adsorptive removal of azithromycin from aqueous solutions using raw and saponin-modified nano diatomite. *Water Sci. Technol.* **80**, 939–949 (2019).

48. Sobhan Ardakani, S., Cheraghi, M., Jafari, A. & Zandipak, R. PECVD synthesis of ZnO/Si thin film as a novel adsorbent for removal of azithromycin from water samples. *Int. J. Environ. Anal. Chem.* 1–18 (2020).

49. Van Tran, T. *et al.* Response surface methodology-optimized removal of chloramphenicol pharmaceutical from wastewater using Cu3 (BTC) 2-derived porous carbon as an efficient adsorbent. *C. R. Chim.* **22**, 794–803 (2019).

50. Saber, W. I. *et al.* Rotatable central composite design versus artificial neural network for modeling biosorption of Cr6+ by the immobilized *Pseudomonas alcaliphila* NEWG-2. *Sci. Rep.* **11**, 1–15 (2021).

51. Rezaei, M., Pourang, N. & Moradi, A. M. Removal of lead from aqueous solutions using three biosorbents of aquatic origin with the emphasis on the affective factors. *Sci. Rep.* **12**, 1–20 (2022).

52. Azari, A., Nabizadeh, R., Nasseri, S., Mahvi, A. H. & Mesdaghinia, A. R. Comprehensive systematic review and meta-analysis of dyes adsorption by carbon-based adsorbent materials: Classification and analysis of last decade studies. *Chemosphere* **250**, 126238 (2020).

53. Liu, X. *et al.* Banana stem and leaf biochar as an effective adsorbent for cadmium and lead in aqueous solution. *Sci. Rep.* **12**, 1–14 (2022).

54. Selambakkannu, S. *et al.* Modification of radiation grafted banana trunk fibers for adsorption of anionic dyes. *Fibers Polym.* **20**, 2556–2569 (2019).

55. Zaib, Q. & Kyung, D. Optimized removal of hexavalent chromium from water using spent tea leaves treated with ascorbic acid. *Sci. Rep.* **12**, 1–14 (2022).

56. Maniyazagan, M., Chakraborty, S., Pérez-Sánchez, H. & Stalin, T. Encapsulation of triclosan within 2-hydroxypropyl-β-cyclodextrin cavity and its application in the chemisorption of rhodamine B dye. *J. Mol. Liq.* **282**, 235–243 (2019).

57. Ali, I., Khan, T. A. & Hussain, I. Treatment and remediation methods for arsenic removal from the ground water. *Int. J. Environ. Eng.* **3**, 48–71 (2011).

58. Mirzaei, N. *et al.* Modified natural zeolite using ammonium quaternary based material for Acid red 18 removal from aqueous solution. *J. Environ. Chem. Eng.* **5**, 3151–3160 (2017).

59. Abdelkhalek, A., El-Latif, M. A., Ibrahim, H., Hamad, H. & Showman, M. Controlled synthesis of graphene oxide/silica hybrid nanocomposites for removal of aromatic pollutants in water. *Sci. Rep.* **12**, 1–22 (2022).

60. Shao, S., Ma, B., Chen, Y., Zhang, W. & Wang, C. Behavior and mechanism of fluoride removal from aqueous solutions by using synthesized $CaSO_4 \cdot 2H_2O$ nanorods. *Chem. Eng. J.* **426**, 131364 (2021).

61. Alnajjar, M. *et al.* Silica-alumina composite as an effective adsorbent for the removal of metformin from water. *J. Environ. Chem. Eng.* **7**, 102994 (2019).

62. Azari, A., Nabizadeh, R., Mahvi, A. H. & Nasseri, S. Integrated Fuzzy AHP-TOPSIS for selecting the best color removal process using carbon-based adsorbent materials: Multi-criteria decision making vs. systematic review approaches and modeling of textile wastewater treatment in real conditions. *Int. J. Environ. Anal. Chem.* 1–16 (2020).

63. Hadavifar, M., Bahramifar, N., Younesi, H. & Li, Q. Adsorption of mercury ions from synthetic and real wastewater aqueous solution by functionalized multi-walled carbon nanotube with both amino and thiolated groups. *Chem. Eng. J.* **237**, 217–228 (2014).

64. Zeng, Z.-W. *et al.* Comprehensive adsorption studies of doxycycline and ciprofloxacin antibiotics by biochars prepared at different temperatures. *Front. Chem.* **6**, 80 (2018).

65. Upoma, B. P. *et al.* A fast adsorption of azithromycin on waste-product-derived graphene oxide induced by H-bonding and electrostatic interactions. *ACS Omega* **7**, 29655–29665 (2022).

Author contributions

All authors contributed to the study conception and design. A.A. and M.M.: Visualization, writing original draft/review, editing and supervision. A.A., K.Y.: Conceptualization, methodology, software, writing-reviewing and editing. G.M. and M.R.M.: Formal analysis, methodology, investigation and writing original draft preparation. R.S. and S.H.: Investigation/writing original draft, formal analysis, data collection and methodology. H.K.: Investigation, software and validation. N.S.F.: Material preparation, data collection and analysis. N.J.: Methodology, writing, review and editing. All authors read and approved the final manuscript.

Competing interests

The authors declare no competing interests.

Additional information

Supplementary Information The online version contains supplementary material available at https://doi.org/10.1038/s41598-022-21551-3.

Correspondence and requests for materials should be addressed to H.K.

Reprints and permissions information is available at www.nature.com/reprints.

Publisher's note Springer Nature remains neutral with regard to jurisdictional claims in published maps and institutional affiliations.